Effect of Fine Structure on Fatigue Resistance Property of Poly(ethylene terephthalate) Tire Cord Fibers

HYUN HOK CHO, KEE HWAN LEE, YUN HYUK BANG

Department of Textile Engineering, College of Engineering, Pusan National University, Pusan, Korea

Received 8 July 1998; accepted 20 May 1999

ABSTRACT: Seven experimental poly(ethylene terephthalate) (PET) fibers were spun and then drawn under different processing conditions (i.e., spinning speed and draw ratio) in such a way that the fibers possessed different long periods but retained the same crystal structure. Wide angle X-ray diffraction, small angle X-ray scattering, loss modulus, initial modulus, and taut tie molecules measurements were used to characterize the fine structure and the physical property of the fibers. The influence of the fine structure on the extensional fatigue behavior of the PET fibers was studied by subjecting them to 120–180 rpm at a repeated extension at 10^4–10^6 cycles. In order to detect the molecular motion of PET with the extensional fatigue, we carried out differential scanning calorimetry, X-ray diffraction, density, and thermoluminescence (TL) experiments. The high temperature TL (above room temperature) intensity decreased with a 10^4 cycle extension but increased with a 10^5 cycle extension. The extent of change in the TL intensity was found to be a function of the long period and loss modulus. © 2000 John Wiley & Sons, Inc. J Appl Polym Sci 78: 90–100, 2000

Key words: poly(ethylene terephthalate) tire cord fiber; fatigue resistance property; taut tie molecules; fraction of taut tie molecules; high temperature thermoluminescence glow curve

INTRODUCTION

Poly(ethylene terephthalate) (PET) fibers are used in many situations in industry (e.g., tire cords and conveyer belts) in which they are subjected to high oscillatory tensile loads, possibly up to a high percentage of their simple tensile strength. The cords in a tire are constantly flexed, extended, and compressed. Therefore, the reinforcing fibers must withstand a large number of such fatiguing cycles without the loss of properties. It is important to improve the fatigue resistance properties of these materials. Great efforts have been made for this purpose and a number of articles have been published on the fatigue resistance property of PET fibers.[1–7] Moreover, the mechanism of the fatigue process and its contribution to fine structural changes are still incompletely understood and need further analysis.

Miyasaka et al.[8–14] developed a new approach by means of the thermoluminescence (TL) method to characterize and evaluate the fatigue and fatigue resistance performance of polymers including PET tire cord. They found that the TL frequency factor S (TL integrated intensity) was very sensitive to the fatigue process of PET tire cords and rubber sheet and that a strong correlation existed between TL intensity and the fatigue process: the TL glow curve was greatly increased in intensity as a result of the cyclic loading. For the same fatigue condition, the change in the TL intensity of crystalline polymers against extension cycles could be possibly utilized as a criterion for fatigue resistance of these polymers. However,

Correspondence to: H. H. Cho.

Journal of Applied Polymer Science, Vol. 78, 90–100 (2000)

Table I Processing Conditions and Physical Properties of Samples

	Sample No.						
	T-1	T-2	T-3	T-4	T-5	T-6	T-7
Spinning speed (m/min)	550	1000	1500	2025	2450	3450	3525
Draw ratio	5.73	4.53	3.07	2.47	2.16	1.74	1.70
Heat-set temp. (°C)	240	240	240	240	240	240	240
Heat-set time (s)	0.2	0.2	0.2	0.2	0.2	0.2	0.2
Intrinsic viscosity (dL/g)	0.89	0.899	0.908	0.913	0.906	0.908	0.900
Tenacity (g/d)	8.4	7.8	7.9	7.7	7.8	7.7	7.1
Elongation (%)	21.4	26.7	21.4	21.0	20.4	20.4	18.4

the samples used in this case were prepared under comparatively high fatigue cycles. It is well known that the fatigue mechanism of the initial stage of fatigue is quite different from that of high fatigue cycles.

In order to obtain more detailed and systematic understanding of the change of fine structure and the molecular motion in the process of fatigue, we studied the changes of TL glow curves, d spacing, and density of PET tire cord fiber with extensional fatigue cycles for various samples with different spinning speeds and draw ratios.

EXPERIMENTAL

Materials

Seven kinds of PET fibers used in this study were provided courtesy of Toyobo Co. Ltd. The processing conditions and data on the mechanical properties of these sample fibers are given in Table I.

Measurements

Wide angle X-ray diffraction (WAXD) experiments were carried out on a Rigaku Denki apparatus (working at 50 kV and 180 mA) using a scintillation counter with a pulse height analyzer. The apparent crystallite size (ACS) was calculated from the half-height width of the (010), (100), and ($\bar{1}$05) diffraction profiles using Scherrer's equation.

$$\text{ACS} = K\lambda/B \cos \theta \quad (1)$$

where K is a constant (0.94), λ is the wavelength of the X ray (1.5418 Å), θ is the Bragg's angle, and B is the intrinsic width of the profile measured (radians).

The width B was estimated using the relation $B^2 = B_m^2 - B_s^2$, where B_m and B_s are measured and instrumental width, respectively. The degree of orientation was calculated from the half-height width of the (100) intensity profile along the Debye ring.

In small angle X-ray scattering (SAXS) experiments the intensity was measured as the same as that for WAXD. The long period (L) was calculated using the following equation from the angle of scattering at the peak maximum x (radians).

$$L = \lambda/x \quad (2)$$

The density was measured at 23°C using a density gradient tube consisting of a mixture of carbon tetrachloride and ethanol. The apparent crystallinity (X) was calculated from the density using the following equation:

$$X = \frac{(d - d_a)}{(d_c - d_a)} \times 100 \quad (3)$$

The crystalline density (d_c) was 1.455 g/mL and the amorphous density (d_a) was 1.335 g/mL.[15]

In the dynamic viscoelasticity measurements, the loss modulus (E'') curves were measured as a function of temperature using a Rheograph from Toyoseiki Co. Ltd. The peak maximum temperature of the α_a dispersion related to the amorphous phase and the half-height width of the E'' peak were measured. The initial modulus (E) was calculated with a length of 50 mm, a 25°C temperature, 65% RH, and 110-Hz frequency according to eq. (4).

$$E = [(L + L_d) \cdot 2/V] \times (\Delta F/\Delta L) \times 3.2 \text{ exp } 8 \quad (4)$$

where V is the sample volume (mL), L is the sample length (cm), L_d is the length change (cm), ΔF is the stress after oscillation (g), and ΔL is the length change after oscillation (cm).

The molecular weight with extension fatigue was calculated using eq. (5) from the intrinsic viscosity as measured in metacresol at 25°C.

$$[\eta] = K \times M^{\alpha} \tag{5}$$

where $[\eta]$ is the intrinsic viscosity, K is the constant (0.77×10^{-3} mL/g), M is the viscosity molecular weight, and α is the constant (0.94).

The thermal behavior with the extensional fatigue was measured by differential scanning calorimetry (DSC). The samples each weighed 5 mg, and the heating rate was 10°C/min. The repeated extension fatigue test was carried out under a cyclic extension of 2% with a frequency of 2–3 Hz at room temperature.

The fraction of taut tie molecules (TTMs) can be calculated by the Peterlin[16] and microfibril[17] model. The model proposed by Peterlin[16] is a simple series parallel model with the following structural unit element for uniaxially orientated polymer samples:

C	
TTM	A

where TTM is the taut tie molecules, A is the nonstretched molecular proportion of the noncrystalline region, and C is the crystalline material.

Assuming a uniform distribution of TTM over the cross section of the noncrystalline regions and if $(L_{(\bar{1}05)}/L)$ is used as the linear degree of order, the following equation for the axial Young's modulus E is valid:

$$E = E_c(\beta + (1 - \beta)E_a/E_c) \div (1 - (L_{\bar{1}05}/L)(1 - \beta)(1 - E_a/E_c)) \tag{6}$$

where E_a is the axial modulus of a completely amorphous sample and E_c is the axial modulus of a single crystal sample. Provided $E_a \ll E_c$ and knowing E and $(L_{(\bar{1}05)}/L)$, the fraction β of TTM can be estimated as follows[18]:

$$\beta = E(1 - L_{\bar{1}05}/\mathrm{L})/(\mathrm{E_c}(1-\mathrm{E}(\mathrm{L}_{(\bar{1}05)}/\mathrm{L})/\mathrm{E_c})) \tag{7}$$

The microfibril model assumes that the polymer structure is divided by ordered and disordered regions and the modes of molecules in the disordered region are chain ends, loops, coiled, tangled, and stretched segments with the latter connecting neighboring crystallites.

The elastic compliance $1/E$ of a series of oriented crystallites and noncrystalline regions can be defined in terms of E_c and E_a.

$$\frac{1}{E} = \frac{d\varepsilon}{d\sigma} = \alpha \frac{d\varepsilon_c}{d\sigma} + (1 - \alpha) \frac{d\varepsilon_a}{d\sigma} = \frac{\alpha}{E_c} + \frac{1 - \alpha}{E_a} = \frac{\alpha}{E_c} + \frac{1 - \alpha}{\beta \cdot E_c + (1 - \beta)E_u} \tag{8}$$

where α is the volume crystallinity, ε is the elongation, σ is the tension, E_c is the chain modulus, and E_u is the axial modulus of unoriented chains.

With $E_u \ll E_c$ the equation yields

$$E \approx E_c \frac{\beta}{1 - \alpha(1 - \beta)} \tag{9}$$

With the inferiority of the fiber modulus E compared with E_c, $E < E_c$, the fraction β of the TTM follows:

$$\beta = \frac{(1 - \alpha)\left(\frac{E}{E_c}\right)}{1 - \alpha \frac{E}{E_c}} \tag{10}$$

In TL measurements, the glow curve was measured above room temperature as a function of temperature with a photomultiplier: samples were heated from 20 to about 180°C at a rate of 6°C/min and the measured glow curves were standardized by the sample weight.

RESULTS AND DISCUSSION

Fine Structure

The XRD photographs in Figure 1 show that the degree of crystalline orientation is high in all the samples. This may be easily explained by taking

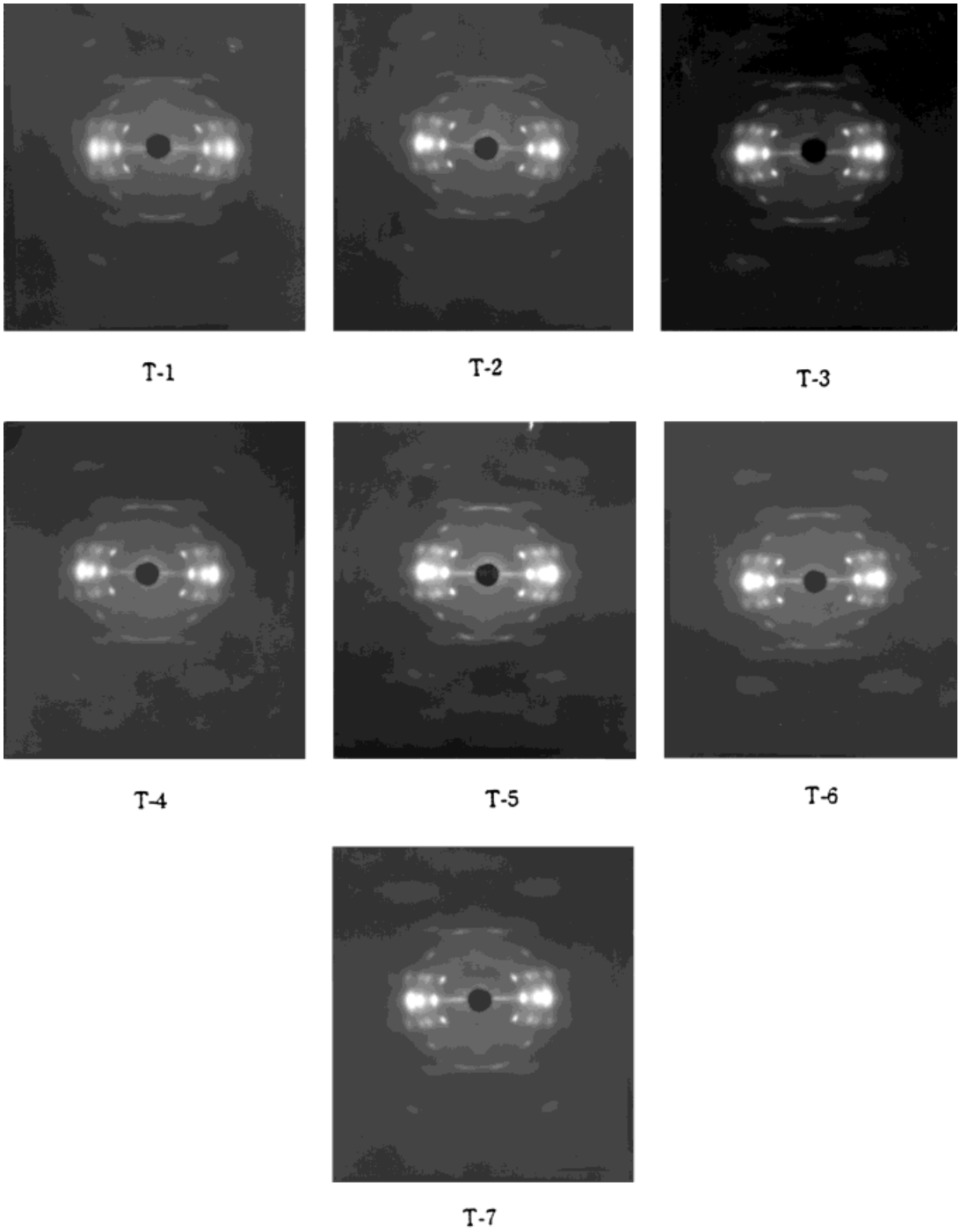

Figure 1 Wide angle X-ray photographs of PET fibers. See Table I for the naming of each sample.

into consideration the data on the spinning speed and the draw ratio as shown in Table I.

Figure 2 shows meridional SAXS intensity curves for sets of PET fibers. One can see changes in the position of the maximum peak with increasing spinning speed (i.e., the long period decreased with increasing spinning speed). It should be noted that all of these samples were heat treated under the same conditions and the annealing temperature dependence of the long

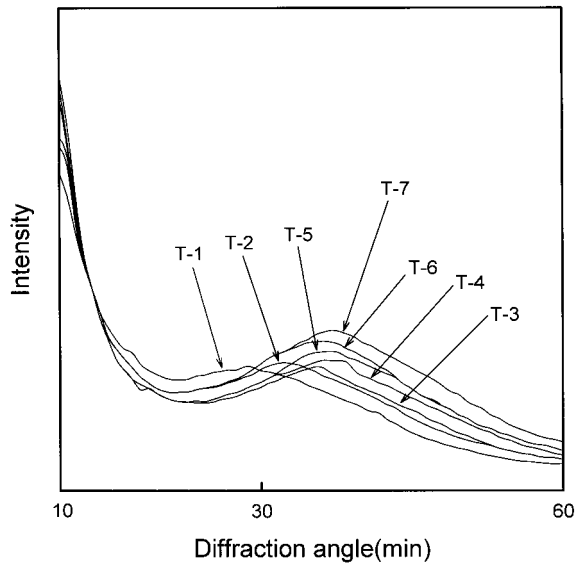

Figure 2 SAXS curves of PET fibers. The sample number is indicated.

period is a well-known fact. The difference in SAXS intensity curves can be seen not only in the maximum peak but also in the intensity itself: the intensity tends to increase with increasing spinning speed. These differences in SAXS should be related to the difference in the crystallization processes: because the as-spun fibers were almost amorphous, the crystallization took place during and after drawing at low spinning speed while the crystallization was induced during spinning at high spinning speed, according to a mode of oriented crystallization. Thus, the long period structure is mainly formed during drawing spun fibers at low spinning speed but it is also formed during spinning spun fibers at high spinning speed. The increase in the SAXS intensity with increasing spinning speed was observed at comparatively high spinning speed and it was considered to be along the same lines as the results obtained in high speed spinning experiments carried out by Shimizu et al.[19]

Figure 3 shows the temperature dependence of the loss modulus (E'') for some sample fibers. The dispersions at around 120°C are the noncrystalline dispersion associated with the micro-Brownian motion of drawn amorphous chains.[20] As the spinning speed increases, the E'' peak, maximum T_α shifts to a lower temperature and the half-height width of the peak decreases, indicating that the mobility of the amorphous chains is larger in spun samples at higher spinning speeds.

The α_a dispersion peak temperature and the half-height width are plotted against the long period in Figure 4. These plots indicate that the increase of noncrystalline orientation in the sample and the increase in the long period are intimately related. These fine structural data for seven kinds of samples are summarized in Table II.

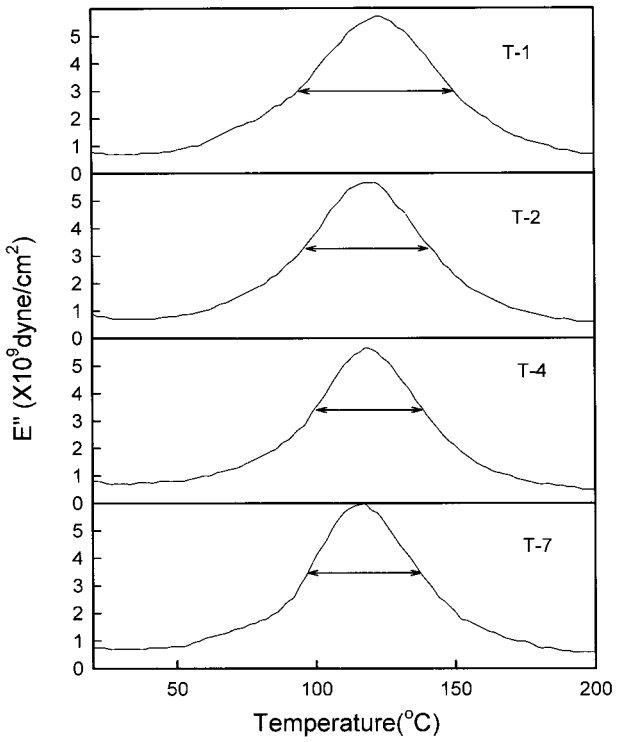

Figure 3 The temperature dependence of the loss modulus (E''). The sample number is indicated.

High Temperature TL Glow Curves

Figure 5 shows the high temperature TL glow curves of the PET fibers. All the samples exhib-

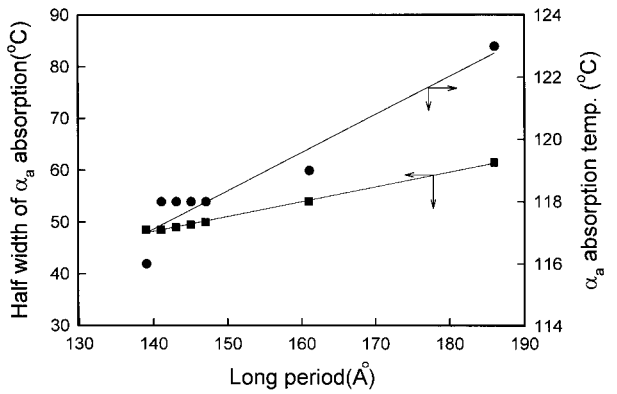

Figure 4 The correlation between the T_α absorption and the long period.

Table II Structural Characteristics of Samples

	Sample No.						
	T-1	T-2	T-3	T-4	T-5	T-6	T-7
d Spacing (Å)							
(010)	5.09	5.09	5.09	5.09	5.09	5.09	5.09
(100)	3.49	3.49	3.49	3.50	3.49	3.49	3.49
($\bar{1}$05)	2.11	2.11	2.11	2.11	2.11	2.11	2.11
Crystallite size (Å)							
(010)	50	49	47	47	50	49	55
(100)	34	33	33	34	33	33	37
($\bar{1}$05)	79	72	67	67	67	67	72
Degree of orientation (%)	94	93	94	94	93	94	95
Long period of SAXS (Å)	186	161	147	141	143	145	139
Degree of crystallinity (%)	48	46	43	44	44	44	44
T_α (°C)	123	119	118	118	118	118	116
Half-width of T_α (°C)	61.5	54.0	50.0	48.5	49.0	49.5	48.5

ited a glow peak with a maximum at 75–80°C and a weak peak on the higher temperature side, making the glow curve asymmetrical.

Figure 6 shows the TL glow curve and loss modulus E'' as a function of temperature for sample T-1 compared with the undrawn sample in order to discuss the TL glow curve in detail. In the undrawn PET the loss modulus peak, E'' maximum, corresponds to the glass transition temperature, T_g; as shown in Figure 6, the undrawn amorphous sample exhibits a very narrow E'' peak at 75°C. In the drawn PET the α peak shifts to a higher temperature as is observed for sample T-1, which has a distinctly measurable crystallinity (Table II). Note that in the undrawn amorphous sample the maximum temperature of the TL peak almost coincides with that of the E'' peak. This suggests that the electron detrapping for the TL glow is triggered by the onset of the α mode relaxation of the amorphous regions.[13] In addition to this main TL peak, a weaker peak appears at above 80°C in all spun and drawn samples (i.e., spinning speed and drawing change the TL glow curve of a single peak to that of double peak). This phenomenon shows that an additional trap site population appeared during

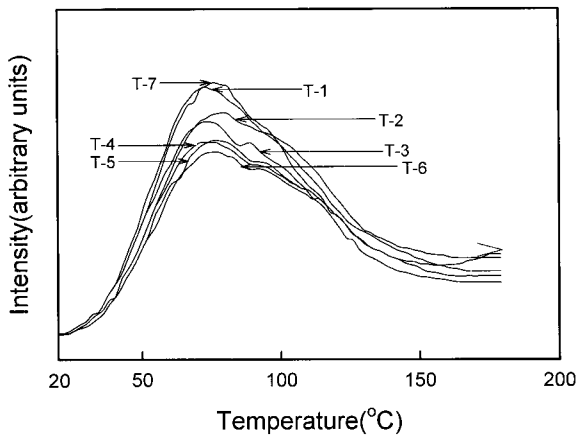

Figure 5 The high temperature TL glow curves of PET tire cord fibers. The sample number is indicated.

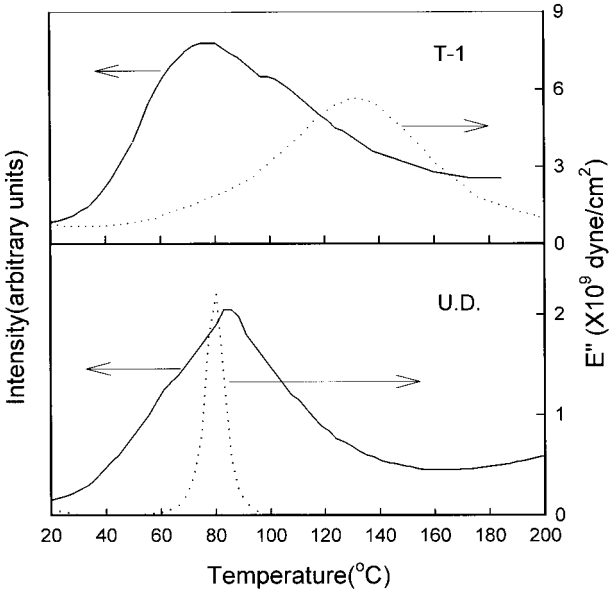

Figure 6 The (—) TL glow curve and (· · ·) loss modulus E'' as a function of temperature for the T-1 sample and undrawn (U.D.) sample.

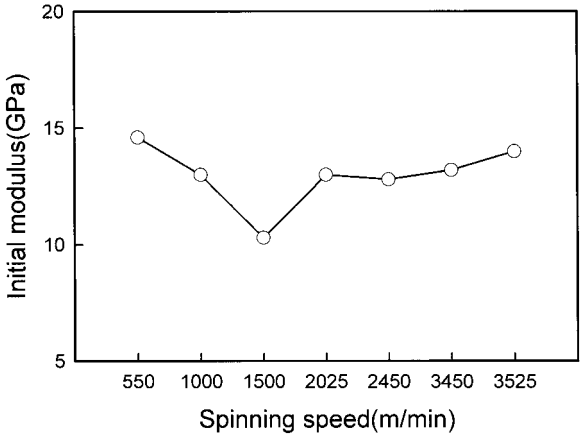

Figure 7 The change of the initial modulus with various spinning speeds.

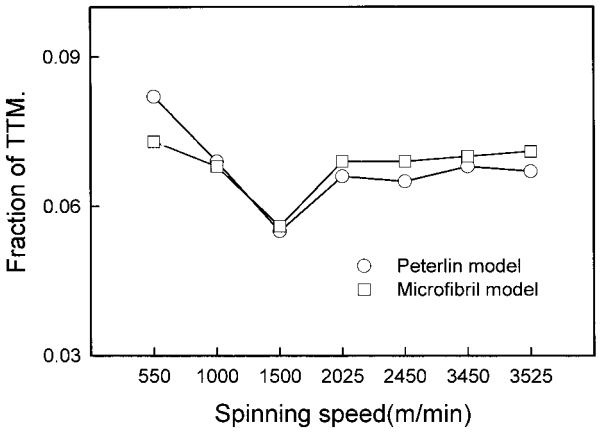

Figure 8 The fraction of the TTMs with various spinning speeds.

the course of these processes, making the TL glow curve asymmetrical. The additional trap sites may be related to the oriented amorphous phase and the interface region of the crystalline and amorphous phases.

Initial Modulus and Fraction of TTM

Figure 7 shows the change of the initial modulus as a function of spinning speed. The initial modulus decreased up to the spinning speed of 1500 m/min because of the decrease of the draw ratio with the increase of spinning speed, but it increased gradually above the spinning speed of 1500 m/min. By comparing the initial modulus of 3500 m/min with the 550 m/min spinning speed, we found that the initial moduli were similar to each other. This suggests that at the high spinning speed (3500 m/min) it is possible to produce PET tire cord yarn with a high modulus.

Figure 8 shows the fraction of TTMs calculated by the Peterlin[16] and microfibril[17] model as a function of spinning speed. The change of the TTM fraction with spinning speed shows a tendency similar to the initial modulus. Modulus is mainly determined by the fraction of TTMs between crystallites in the same fibril. These molecules connect crystallites that are neighbors in one fibril through a noncrystalline region and have the same axial modulus as a chain section in a crystallite. It is shown that values of β between two models are different because of calculations using different crystallinity: the linear degree of order by the Peterlin model[16] and the volume crystallinity by the microfibril model.[17] Figure 9 shows the initial modulus as a function of the fraction of TTM, and the initial modulus increased with the increase of the fraction of TTMs. It is indicated that the initial modulus depends on the fraction of TTMs.

Change of TL Glow Curve by Repeated Extension Fatigue

According to the phenomenological interpretation of the TL glow curve by Randall and Wilkins,[21] the TL intensity L at any time t is given by the product of the ion recombination rate and the luminescence constant α (the probability of proton emission from each recombination).

$$L = -\alpha\left(\frac{dn}{dt}\right) \tag{11}$$

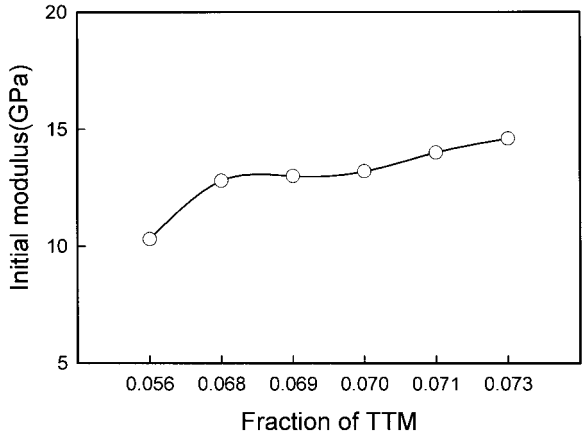

Figure 9 The change of the initial modulus with the fraction of TTMs.

and for the first-order ion recombination

$$\frac{dn}{dt} = -Kn \tag{12}$$

where n is the number of trapped ion pairs at time t and K is a recombination rate constant. If the trapped charges were released by purely thermal activation from a trap, K might be expressed as follows:

$$K = S \exp\left(-\frac{E}{kT}\right) \tag{13}$$

where E is the activation energy (trap depth) and S is the attempt to escape frequency. Accordingly, eq. (11) is

$$L = -\alpha\left(\frac{dn}{dt}\right) = \alpha S n \exp\left(-\frac{E}{kT}\right) \tag{14}$$

where

$$n = n_0 \exp\left[-S \int_0^t \exp\left(-\frac{E}{kT}\right) dt\right] \tag{15}$$

where n_0 is the number of trapped ion pairs at the starting point of warming ($t = 0$).

From eq. (14), the TL glow intensity depends on the number of trapped electrons n_0 during irradiation and the activation energy E for detrapping of the electrons, which is usually triggered by the molecular motion during heating and the attempt to escape frequency S. More trapped electrons and a larger S both increase the TL glow intensity, while a larger E decreases the TL glow ability and tends to shift the peak to a higher temperature.

Figure 10(a) shows TL glow curves of sample T-1 with a long periods of about 186 Å before and after repeated extension fatigues of 10^4 and 10^5 cycles. In this case the TL glow intensity was reduced with a 10^4 repeated extension and at the same time the glow peak shifted to a higher temperature. Cyclic extension of PET fibers generally causes two opposite effects on the TL glow ability: the decrease in the trap site number due to the strain hardening and the increase in the trap site number due to the introduction of defects.[9] Thus, the change in the TL glow ability with cyclic extension increases in some cases and decreases in other cases according to the

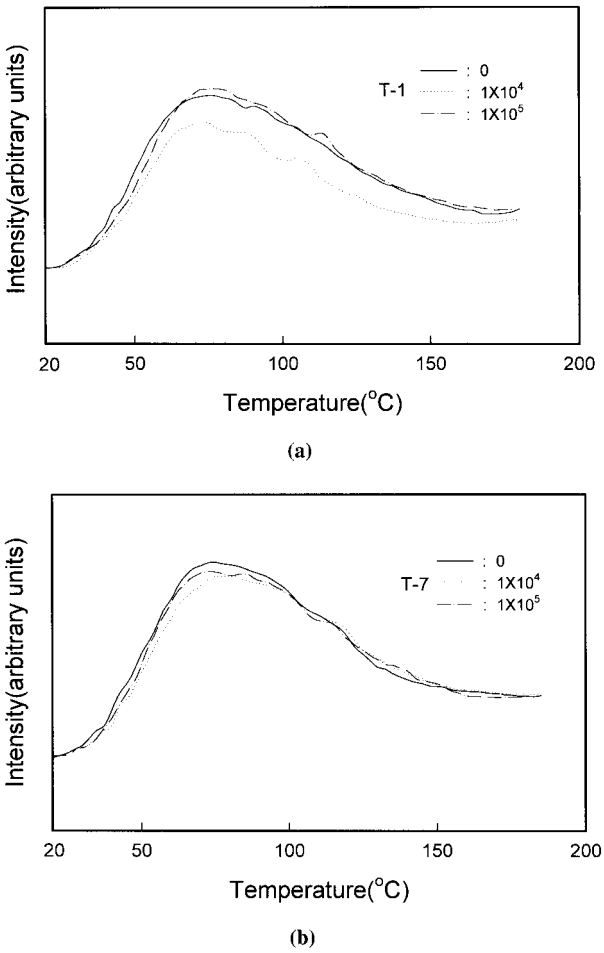

Figure 10 (a) The high temperature TL glow curves of the T-1 sample before and after repeated extension fatigue tests at room temperature. (b) The high temperature TL glow curves of the T-7 sample before and after repeated extension fatigue tests at room temperature.

conditions. It was also shown that the effect of defects on TL glow seemed to be more recoverable than that of strain hardening when the samples were kept standing at room temperature, as revealed by the noticeable decrease in TL glow ability measured as a function of aging time after the finishing of cyclic extension. In almost all tire yarns the TL glow ability of the sample fatigued with cyclic extension, measured after a long period of aging, was less than that measured before cyclic extension. The result shown in Figure 10(a) indicates that the strain hardening effect is stronger than the effect of defects. Figure 10(a) also shows the results of the same sample that suffered from a 10^5 cyclic extension. In this case, the TL glow ability slightly increased with repeated extensions. This

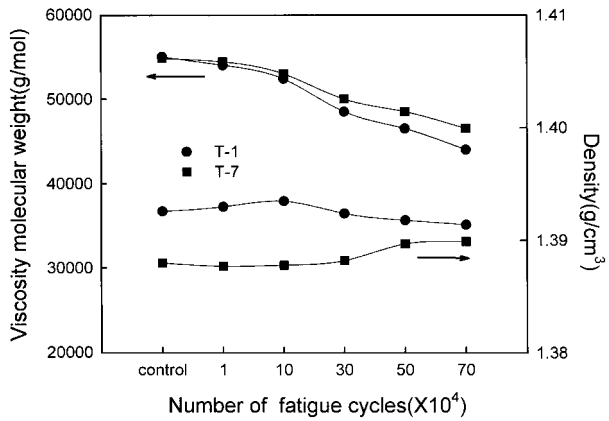

Figure 11 The change of the viscosity molecular weight and density with repeated extension fatigues.

indicated that the increase in the number of cyclic extensions from 10^4 to 10^5 certainly enhanced the effect of defects introduced by the cyclic extensions. These results certainly support our proposal on the two effects of fatigue on TL glow ability and indicate that the strain hardening effect is predominant at an early stage of cyclic extension and is followed by the effect of defects at a later stage. This is very understandable when we consider how the stress–strain curve changes with cyclic extension: one can see that the most remarkable change in the stress–strain relation is always induced by the first extension, and the second remarkable change is induced by the second extension. This change in the stress–strain relation is strain hardening. This means that strain hardening occurs at an early stage of repeated extensions and the rate of hardening must decrease with an increasing number of repeats of the extension. On the other hand, the situation of the defect origination is quite different. There is no doubt that the increase in the number of repeats is always favorable for the increase in the number of defects: the strain hardening must help the source of the defects, because of the decrease in the relaxation time, and the number of defects should increase the average possibility of the occurrence of defects by the number of repeats. The possibility must be a function of the number of repeats. However, it is reasonable to suppose that the number of defects continues to increase, being cumulative, but even at a larger number of repeats the strain hardening almost stopped increasing.

Figure 10(b) shows TL glow curves of sample T-7 with a long period of about 139 Å before and after repeated extension fatigues of 10^4 and 10^5 cycles. The general features are the same as those described for Figure 10(a), but the decrease in the TL glow intensity is smaller than in the sample T-1 with a larger long period (186 Å). It can be predicted that the fatigue resistance property for sample T-7 with a smaller long period is better than that of sample T-1 with a larger long period, which was revealed by many authors.[22–25]

Changes of Fine Structure by Repeated Extension Fatigues

Figure 11 shows the changes of viscosity molecular weights and density with repeated extension fatigues. The viscosity molecular weights gradu-

Table III Change of Structural Characteristics of Samples with Number of Repeated Extension Fatigues

Sample No.	No. Repeated Extension Fatigues ($\times 10^4$)	Degree of Orientation (%)	*d* Spacing (Å)		Crystallite Size (Å)	
		(100)	(010)	(100)	(010)	(100)
T-1	Control	94.00	5.09	3.49	50	34
	1	94.70	5.08	3.48	49	35
	10	94.72	5.07	3.47	49	35
	30	94.74	5.07	3.48	49	34
	70	93.98	5.08	3.48	50	35
T-7	Control	95.00	5.09	3.49	55	37
	1	94.94	5.03	3.45	55	38
	10	94.70	5.02	3.43	55	38
	30	93.55	5.02	3.43	55	38
	70	93.83	5.03	3.43	54	37

ally decreased with the increase of the number of repeated extensions caused by chain scission of molecules. By comparing T-7 with T-1, T-7 with a smaller long period had less changes in the molecular weights with the repeated extensions than T-1, because it took less stress and better uniformly distributed stress in the molecular chain. But in case of density, a change with the number of repeated extension fatigues scarcely occurred. According to the increase of fatigue cycles, we expected that a decrease of density from the increase of defects caused by chain scission was shown in the change of molecular weights, but the gradual decrease of density was not observed. So, we considered that the strain hardening effects on the amorphous region continuously occurred with the increase of fatigue cycles, because density scarcely decreased in spite of chain scission.

Table III shows the changes of the crystalline region according to the number of repeated extensions, which is calculated by the WAXD profile [i.e., crystalline orientation of (100), d spacing, and crystallite size]. In rayon tire cord, Ono[26] reported that the sliding of the crystal plane and the decrease of crystallinity occurred with an increase of the number of extension fatigues, but the changes of the crystalline region with the cyclic extension scarcely occurred in this study. Figures 12 and 13 show the DSC thermograms of the samples with repeated extensions. The melting temperature scarcely changed with repeated extension fatigues. Table III shows that the fine structure with extension fatigue was mainly changed in the amorphous region.

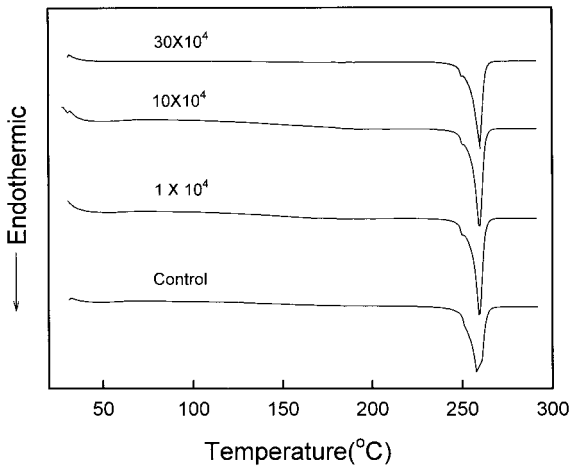

Figure 12 DSC thermograms of the T-1 sample with repeated extension fatigues.

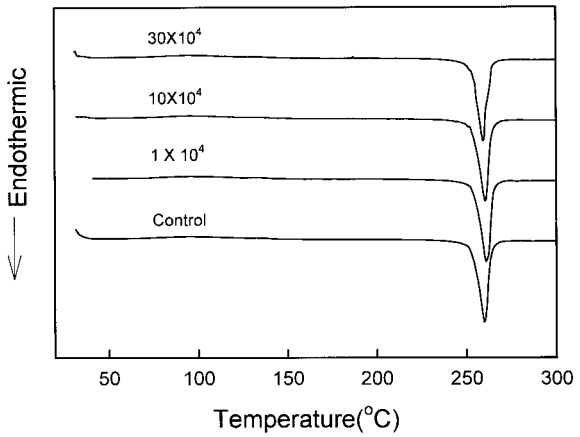

Figure 13 DSC thermograms of the T-7 sample with repeated extension fatigues.

CONCLUSIONS

It would appear from our results that there was a change of fine structure on cyclic extension in PET tire cord. The change of fine structure mainly occurred in the amorphous region, and it was due to two effects occurring at the same time: an increase of defects caused by chain scission and the strain hardening effect. The strain hardening effect was predominant at the early stage of cyclic extension and was followed by the effect of defects at a later stage. The fatigue resistance property for sample T-7 with a smaller long period was better than that of sample T-1 with a larger long period.

REFERENCES

1. Aitken, R. G.; Griffith, R. L.; Little, J. S.; Mclellan, P. W. Rubber World 1965, 151(2), 58.
2. Hearle, J. W. S. J Mater Sci 1967, 2, 474.
3. Hearle, J. W. S.; Vaughm, E. A. Rheol Acta 1970, 9(1), 76.
4. Bunsell, A. R.; Hearle, J. W. S. J Appl Polym Sci 1974, 18, 267.
5. Fu-Min, L.; Goswami, B. C.; Spruiell, J. E.; Duckett, K. E. J Appl Polym Sci 1985, 30, 1859.
6. Winkler, E. M. Text Res J 1991, 61, 441.
7. Pecorini, T. J.; Hertzberg, R. W. Polymer 1993, 34, 5053.
8. Miyasaka, K.; Hashimoto, T. Sen-i Gakkaishi 1982, 38, 46.
9. Liu, J. H.; Danno, T.; Hashimoto, T.; Miyasaka, K.; Mitsuishi, Y. Sen-i Gakkaishi 1984, 40, 57.
10. Hiyama, K.; Miyasaka, K. Sen-i Gakkaishi Prepr 1985, s-78.

11. Liu, L. B.; Miyasaka, K. Sen-i Gakkaishi Prepr 1986, s-12.
12. Liu, L. B.; Sumita, M.; Miyasaka, K. Polym Prepr 1987, 26, 2429.
13. Liu, L. B.; Hiyama, K.; Miyasaka, K. Polymer 1988, 29, 286.
14. Miyasaka, K. Sen-i Gakkaishi 1990, 46, 408.
15. Daubeny, P.; Bunn, C. W.; Brown, C. J. Proc R Soc Lond Ser A 1988, 226, 286.
16. Peterlin, A. In Ultra High Modulus Polymers; Ciferri, A.; Ward, I. M., Eds.; Applied Science Publishers: London, 1979.
17. Prevorsec, D. C.; Harget, P. J.; Shama, R. K.; Reimschuessel, A. C. J Macromol Sci Phys 1973, B8, 127.
18. Schultze-Gebhardt, F.; Dormagen/FRG, Chemiefasern/Textilindustrie 1990, 40/92, E49.
19. Shimizu, J.; Okui, N.; Kikutani, T. Sen-i Gakkaishi 1981, 37, T-135.
20. Tompson, A. B.; Woods, P. W. Trans Faraday Soc 1956, 52, 1383.
21. Randall, J. T.; Wilkins, M. H. F. Proc R Soc Lond Ser A 1945, 184, 366.
22. Meredith, R. J Text Inst 1954, 45, T30.
23. Morton, W. E.; Hearle, J. W. S. Physical Properties of Textile Fibers, 3rd ed.; The Textile Institute: Manchester U.K., 1993; Chap. 18.
24. Gibson, A. G.; Davies, G. R.; Ward, I. M. Polymer 1988, 19, 683.
25. Mitsuishi, Y.; Nagai, A.; Hasegawa, K. Sen-i Gakkaishi Prepr 1988, s-154.
26. Taiya Ono, R.; Maeda, H.; Fujiwara, S. Sen-i Gakkaishi 1965, 19, 435.